



Joint Effects of Co-Channel Interferences and Pointing Errors on Dual-Hop Mixed RF/FSO Fixed-Gain and Variable-Gain Relaying Systems

Junrong Ding , Dongpeng Kang , *Member, IEEE*, Xiaolong Xie, Ling Wang, Liying Tan, and Jing Ma

Abstract—The performance of a dual-hop mixed radio frequency (RF)/free space optical (FSO) system with co-channel interferences (CCIs) is studied for both fixed-gain and variable-gain amplify-and-forward (AF) relaying scenarios. The RF link and interference link undergo the κ - μ shadowed fading and the FSO link experiences the Fisher-Snedecor \mathcal{F} distribution with pointing errors. For the considered system, we derive new closed-form expressions for the probability density function (PDF), cumulative distribution function (CDF), and average bit error rate (BER) of the end-to-end signal-to-interference-plus-noise ratio (SINR). In addition, efficient numerical expressions for the ergodic capacity are also obtained. Moreover, the asymptotic expressions for the CDF and average BER are derived. Our results can be regarded as a generalization of the previous results. Finally, numerical and simulation results are presented to verify the correctness of the proposed expressions.

Index Terms—Mixed RF/FSO relaying, co-channel Interferences, pointing errors, average bit error rate, ergodic capacity.

I. INTRODUCTION

WITH the increasing demands for the bandwidth in wireless networks, millimeter wave (mmWave) bands have attracted much attention in the design of 5G networks [1]. However, mmWave cellular communication depends heavily on the propagation environment. First, power transmitted over long distances may be attenuated due to various factors such as absorption and atmospheric conditions; Second, signals cannot penetrate through obstacles such as buildings, vehicles, and trees, etc. In order to extend the coverage area, improve signal quality, enhance the communication link reliability, and combat the blockage effects, a practical solution is to deploy

Manuscript received 10 January 2023; accepted 15 January 2023. Date of publication 6 February 2023; date of current version 10 February 2023. This work was supported in part by the National Natural Science Foundation of China under Grant 61705053, in part by China Postdoctoral Science Foundation under Grant 2016M600249, and in part by the Heilongjiang Provincial Postdoctoral Science Foundation, Fundamental Research Funds for the Central Universities through the Major Key Project of PCL under Grant PCL2022A02-2. (*Corresponding author: Dongpeng Kang.*)

Junrong Ding, Dongpeng Kang, Liying Tan, and Jing Ma are with the National Key Laboratory of Tunable Laser Technology, Harbin Institute of Technology, Harbin 150001, China (e-mail: jrdinghit@stu.hit.edu.cn; dongpeng.kang@hit.edu.cn; tanly@hit.edu.cn; majing@hit.edu.cn).

Xiaolong Xie is with the Peng Cheng Laboratory, Shenzhen 518000, China (e-mail: x_xiaolong@yeah.net).

Ling Wang is with the School of Internet, Anhui University, Hefei 230039, China (e-mail: wangling199059@163.com).

Digital Object Identifier 10.1109/JPHOT.2023.3238205

relays along intermediate paths. In addition, the congestion of the backhaul networks has raised significant concern in the deployment of mmWave cellular networks [2], [3]. Recently, due to its immunity to interference, license-free spectrum, and high data rate, free space optical (FSO) communication technology has been considered as a promising solution for low-cost backhaul construction [4], [5]. In this perspective, mixed RF/FSO relaying systems represent an effective scenario for wireless networks.

Our research focuses on the performance of dual-hop RF/FSO relaying systems (e.g., outage probability (OP), average bit error rate (BER), and ergodic capacity (EC)). In fact, many studies on the performance of the kind of systems have been reported [6], [7], [8], [9], [10], [11], [12], [13], [14], [15], [16], [17], [18], [19]. For the FSO link, joint effects of atmospheric turbulence and pointing errors were studied. The atmospheric turbulence induced fading is mainly modeled by the log-normal [4], gamma-gamma (GG) [4], α - μ [20], double generalized gamma (double GG) [21], M [22], and Fisher-Snedecor \mathcal{F} [23] distributions. Compared with other distributions, the Fisher-Snedecor \mathcal{F} distribution overcomes the limitation due to mathematical complexity. Moreover, this distribution also better describes weak-and-strong irradiance fluctuations. The pointing error models include the Beckmann [24], approximate Beckmann [25], Rayleigh [26], Hoyt [27], and Rician [28] distributions. The Fisher-Snedecor \mathcal{F} distribution with Rayleigh pointing errors. Finding combined statistics of turbulence and pointing errors becomes mathematically intractable when general models are considered. To this end, the Fisher-Snedecor \mathcal{F} distribution with approximate Beckmann pointing errors was introduced [19]. We note that single-link FSO system [29], dual-hop AF relaying-based FSO system [30], and dual-hop AF relaying-based mixed RF/FSO system [19] over Fisher-Snedecor \mathcal{F} Turbulence channels with pointing errors were studied and reported.

Moreover, in the implementation of commercial FSO systems, the intensity modulation and direct detection (IM/DD) with on/off keying (OOK) has been widely used due to its simplicity and low cost. However, one of the main flaws of OOK is the requirement for adaptive detection threshold to achieve its optimal error rate performance. In contrast, the subcarrier intensity modulation (SIM) avoids the need for the adaptive threshold, so it has broad application prospects [31], [32], [33], [34]. Recently, SIM is widely implemented into the relays to modulate the intensity of the optical carrier.

TABLE I
SUMMARY OF STUDIES OF CO-CHANNEL INTERFERENCE IN DUAL-HOP MIXED RF/FSO SYSTEMS

Ref.	RF link	Interference link	FSO link	Relaying system	Metrics
[41]	Nakagami- m	Nakagami- m	GG	DF	OP
[42]	Rayleigh	Rayleigh	\mathcal{M}	AF, fixed gain, variable gain	OP, BER
[43]	Nakagami- m	Nakagami- m	GG	AF, fixed gain	OP
[20]	η - μ	Rayleigh	α - μ	AF, fixed gain	OP, BER, EC
[21]	Nakagami- m	Nakagami- m	Double GG	AF, fixed gain, variable gain	OP, BER
[2]	Nakagami- m	Nakagami- m	Double GG	AF, variable gain	OP, BER, EC
[44]	Rayleigh	Nakagami- m	α - μ	AF, fixed gain	OP, BER, EC
[45]	Rayleigh	Rayleigh	\mathcal{M}	DF	OP, BER, EC
[46]	Nakagami- m	Nakagami- m	\mathcal{M}	DF	OP, EC
This work	κ - μ shadowed	κ - μ shadowed	Fisher-Snedecor \mathcal{F}	AF, fixed gain, variable gain	OP, BER, EC

On the RF side, small-scale fading is mainly considered. The Rayleigh, Rician, and Nakagami- m distributions are used to describe multipath fading scenarios. In fact, in wireless networks, the RF signals are adversely affected by shadowing caused by the user's body [35]. Therefore, a composite fading model that includes multipath fading and shadowing scenarios simultaneously is necessary to be studied. The κ - μ [10], η - μ [10], α - η - κ - μ [36], [37], [38], and Rician shadowed distributions [39] are used to describe the above scenarios. Interestingly, the κ - μ shadowed fading model including the one-side Gaussian, Rayleigh, Nakagami- m , Rician, κ - μ , and Rician shadowed distributions, is a generalized model [40].

In practical scenarios, co-channel interferences (CCIs) due to frequency reuse could severely limit the reception quality, especially on the RF reception [20]. However, in most of the above literatures, the CCIs incorporated in the RF link have been ignored by assuming interference-free relays. Although a handful of models considered CCIs in dual-hop mixed RF/FSO systems, as summarized in Table I, their applications are limited because either they adopt FSO models which are mathematically complex and lead to the difficulty of deriving closed-form expressions, or the RF models may not accurately describe composite multipath/shadowed signal. In particular, when RF and FSO links adopt simple, accurate, and generalized channel models, such as Fisher-Snedecor \mathcal{F} , approximate Beckmann, κ - μ shadowed distributions, the effects of CCIs on dual-hop RF/FSO fixed-gain and variable-gain relaying systems have not been studied. Therefore, the effect of CCIs should be taken into account on the design and implementation of such relaying systems.

Motivated by the aforementioned discussions, we investigate the effects of CCIs on dual-hop mixed RF/FSO amplify-and-forward (AF) relaying systems, where the RF link experiences κ - μ shadowed fading and the FSO link is subject to Fisher-Snedecor \mathcal{F} fading. We also include the effects of pointing errors in our models with the formalism recently derived [19]. In addition, we study systems of both gain mechanisms in the relay, fixed-gain and variable-gain, and compare the performance by assuming the same average gain. This work provides generalized, closed-form formalisms for analyzing systems of this kind when both CCIs and pointing errors are present.

Our main contributions of this work are as follows: For both fixed-gain and variable-gain relaying scenarios, we derive new closed-form expressions for the cumulative distribution function

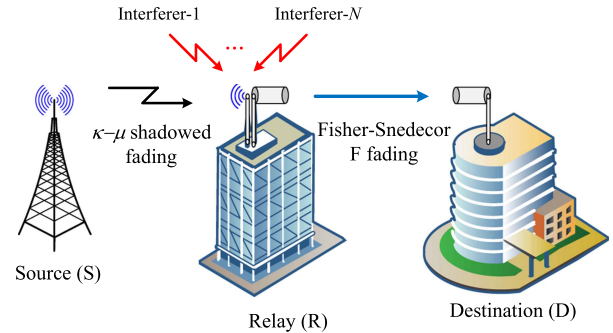


Fig. 1. A dual-hop RF/FSO AF relaying system with co-channel interferences.

(CDF) and probability density function (PDF) of the end-to-end signal-to interference-plus-noise ratio (SINR). Based on the above expressions, we derive new closed-form expressions for the average BER and provide efficient numerical expressions for the ergodic capacity.

The rest of the paper is organized as follows: In Section II, system and channel models are introduced. In Section III, we derive the PDF and CDF of the end-to-end SINR for both fixed-gain and variable-gain relaying scenarios. In Section IV, we investigate the average BER and the ergodic capacity. Section V presents and discusses some numerical and analytical results. Finally, Section VI presents concluding remarks.

II. SYSTEM AND CHANNEL MODELS

We consider a dual-hop mixed RF/FSO AF relaying system with CCIs, as shown in Fig. 1. In the considered system, the source node S communicates with the destination node D via a relay node R, where N sources of RF CCIs exist. In addition, the AF relaying node can convert RF signals into the FSO signal using SIM.

A. RF Channel Model

The received RF signal at the relay node R is expressed as

$$r_{sr} = h_{sr}x + \sum_{i=1}^N h_i x_i + n_{sr}, \quad (1)$$

where x is the information signal with an average power $\mathbb{E}[|x|^2] = P_s$, with $\mathbb{E}[\cdot]$ being the expectation operator; h_{sr} is the κ - μ shadowed fading coefficient; x_i is the interference signal of

the i -th interferer with an average power $\mathbb{E}[|x_i|^2] = P_i$; h_i is the fading coefficient between the i -th interferer and the relay; n_{sr} is the white Gaussian noise with zero-mean and variance of N_0 . The instantaneous SNR in the RF link is $\gamma_1 = \bar{\gamma}_1 |h_{sr}|^2$, where $\bar{\gamma}_1 = \frac{P_s}{N_0}$ is the average SNR. The PDF of γ_1 is given by [40]

$$f_{\gamma_1}(\gamma_1) = \frac{\mu^\mu m^m (1+\kappa)^\mu}{\Gamma(\mu) \bar{\gamma}_1 (m+\kappa\mu)^m} \left(\frac{\gamma_1}{\bar{\gamma}_1}\right)^{\mu-1} e^{-\frac{\mu(1+\kappa)\gamma_1}{\bar{\gamma}_1}} \times {}_1F_1\left(m; \mu; \frac{\mu^2 \kappa (1+\kappa) \gamma_1}{(m+\kappa\mu) \bar{\gamma}_1}\right), \quad (2)$$

where $\Gamma(\cdot)$ is the gamma function; ${}_1F_1(\cdot; \cdot; \cdot)$ is the confluent hypergeometric function ((9.210.1) in [47]). However, ${}_1F_1(\cdot; \cdot; \cdot)$ leads to a very complex mathematical form. To this end, in [48], when μ and m take integer values, the κ - μ shadowed distribution is represented by a finite sum of powers and exponentials, which makes it extremely convenient to calculate. In addition, when the field measurement values are fitted to this distribution, the restriction on integer values for μ and m has little practical impact. The PDF of γ_1 can be rewritten as ((12) in [48])

$$f_{\gamma_1}(\gamma_1) = \sum_{i=0}^M \frac{C_i \gamma_1^{m_i-1}}{(m_i-1)! \Omega_i^{m_i}} e^{-\frac{\gamma_1}{\Omega_i}}. \quad (3)$$

Using (3), (8.4.3.1) in [49], and (2.54) in [50], the CDF of γ_1 can be rewritten as

$$F_{\gamma_1}(\gamma_1) = 1 - \sum_{i=0}^M \frac{C_i}{(m_i-1)!} \text{H}_{1,2}^{2,0} \left[\frac{\gamma_1}{\Omega_i} \middle| (1, 1), (m_i, 1), (0, 1) \right], \quad (4)$$

where $\text{H}_{1,2}^{2,0}(\cdot)$ is the Fox's H function [51].

On the other hand, the relay receives N independently identically distributed (i.i.d.) interfering signals. Assume instantaneous interference-to-noise ratio (INR) follows κ - μ shadowed distribution, i.e., $\gamma_{I,i} \sim (\bar{\gamma}_I, \kappa_I, \mu_I, m_I)$, the total instantaneous INR, $\gamma_I = \sum_{i=1}^N \frac{|h_i|^2 P_i}{N_0}$, follows another κ - μ shadowed distribution with scaled parameters, i.e., $\gamma_I \sim (N\bar{\gamma}_I, \kappa_I, N\mu_I, Nm_I)$, with the PDF given by

$$f_{\gamma_I}(\gamma_I) = \sum_{\ell=0}^{M_X} \frac{C_{X,\ell} \gamma_I^{m_{X,\ell}-1}}{(m_{X,\ell}-1)! \Omega_{X,\ell}^{m_{X,\ell}}} e^{-\frac{\gamma_I}{\Omega_{X,\ell}}}, \quad (5)$$

where $\bar{\gamma}_I = \mathbb{E}[\frac{|x_i|^2 P_i}{N_0}]$ is the average INR per CCI link. The CDF of γ_I is given by

$$F_{\gamma_I}(\gamma_I) = 1 - \sum_{\ell=0}^{M_X} C_{X,\ell} e^{-\frac{\gamma_I}{\Omega_{X,\ell}}} \sum_{t=0}^{m_{X,\ell}-1} \frac{1}{t!} \left(\frac{\gamma_I}{\Omega_{X,\ell}}\right)^t. \quad (6)$$

B. FSO Channel Model

When pointing errors are considered, the FSO link can be modeled by the Fisher-Snedecor \mathcal{F} distribution with the PDF and CDF of the instantaneous SNR (γ_2) given by [19]

$$f_{\gamma_2}(\gamma_2) = \frac{\xi_{\text{mod}}^2}{r\Gamma(a)\Gamma(b)\gamma_2} \times \text{G}_{2,2}^{2,1} \left[\frac{a\varphi\gamma_2^{\frac{1}{r}}}{(b-1)\mu_r^{\frac{1}{r}}} \middle| 1-b, \xi_{\text{mod}}^2+1, a, \xi_{\text{mod}}^2 \right], \quad (7)$$

and

$$F_{\gamma_2}(\gamma_2) = 1 - \frac{\xi_{\text{mod}}^2}{r\Gamma(a)\Gamma(b)} \times \text{H}_{3,3}^{3,1} \left[\frac{a\varphi\gamma_2^{\frac{1}{r}}}{(b-1)\mu_r^{\frac{1}{r}}} \middle| (1-b, 1), (\xi_{\text{mod}}^2+1, 1), (1, \frac{1}{r}), (0, \frac{1}{r}), (a, 1), (\xi_{\text{mod}}^2, 1) \right], \quad (8)$$

where $\text{G}_{2,2}^{2,1}(\cdot)$ is the Meijer's G function [47]; a and b represent turbulence parameters; μ_r is the average electrical SNR, where $r=1$ and $r=2$ represent heterodyne detection (HD) and direct detection (DD), respectively. In particular, $\mu_1 = \mu_{\text{HD}} = \bar{\gamma}_{2(\text{HD})}$; $\mu_2 = \mu_{\text{DD}} = a\varphi(\xi_{\text{mod}}^2+2)(b-2)\bar{\gamma}_{2(\text{DD})}/[(b-1)(a+1)(\xi_{\text{mod}}^2+1)]$, where $\varphi = \xi_{\text{mod}}^2/(\xi_{\text{mod}}^2+1)$; ξ_{mod}^2 is associated with the equivalent beam width w_{Leq} , the standard deviations for the horizontal (σ_x) and the elevation (σ_y) axes, and the fixed boresight errors for the horizontal (μ_x) and the elevation (μ_y) axes. The value of ξ_{mod}^2 increases with the decrease of pointing errors, and $\xi_{\text{mod}}^2 \rightarrow \infty$ when pointing errors are absent.

C. End-to-End Sinr

The end-to-end signal-to-interference plus noise ratio (SINR) at the destination node D can be expressed as [21], [43]

$$\gamma = \frac{\gamma_1 \gamma_2}{\gamma_2 \gamma_I + \gamma_2 + C}, \quad (9)$$

where $C = 1/(G^2 N_0)$. When both fixed-gain and variable-gain relaying systems are assumed to have the same average gain as in [52], the scaling gain at the relay node R can be chosen as $G = 1/\sqrt{\mathbb{E}[|h_{sr}|^2]P_s + \sum_{i=1}^N \mathbb{E}[|h_i|^2]P_i + N_0}$ for the fixed-gain relaying scenario, and $G = 1/\sqrt{|h_{sr}|^2 P_s + \sum_{i=1}^N |h_i|^2 P_i + N_0}$ for the variable-gain relaying scenario, respectively. The end-to-end SINR for variable-gain relaying can be further simplified as

$$\gamma = \frac{\gamma_1 \gamma_2}{\gamma_1 + \gamma_2 + \gamma_2 \gamma_I + \gamma_I + 1} = \frac{\gamma_1^{\text{eff}} \gamma_2}{\gamma_1^{\text{eff}} + \gamma_2 + 1}, \quad (10)$$

where $\gamma_1^{\text{eff}} = \gamma_1/(\gamma_I + 1)$.

III. STATISTICAL CHARACTERISTICS

In this section, the PDF and CDF of the end-to-end SINR are derived for both fixed-gain and variable-gain relaying scenarios.

A. Fixed-Gain Relaying

1) Cumulative Distribution Function:

a) *Exact Analysis:* The CDF of γ of the considered dual-hop RF/FSO fixed-gain relaying system can be obtained as (11) shown at the bottom of the next page, where $\text{H}_{3,3,3,3}^{3,3,3,3}(\cdot, \cdot)$ is the bivariate Fox's H function.

Proof: See Appendix A.

Note that when $\xi_{\text{mod}}^2 \rightarrow \infty$, (11) is reduced to the CDF expression without pointing errors.

b) *Asymptotic Analysis:* For infinite $\bar{\gamma}_1$ and μ_r , using (1.8.4) in [51] and $e^{-\frac{\gamma}{\Omega_i}} \approx 1 - \frac{\gamma}{\Omega_i}$, the asymptotic CDF can

be obtained as (12) shown at the bottom of this page, where

$$\Delta_1 = \frac{a\varphi C^{\frac{1}{r}}}{(b-1)\mu_r^{\frac{1}{r}}\Omega_i^{\frac{1}{r}}} \text{ and } \Delta_2 = \frac{\Omega_i}{q\Omega_i+1}.$$

When the interference power is scaled with the transmitted power, the INR tends to infinity as the SNR tends to infinity. Under this assumption, at high SNRs, the presence of CCIs at relay node R results in the occurrence of BER floors and capacity ceilings, which reflects the fact that the diversity order is $G_d = 0$.

2) *Probability Density Function*: By differentiating (11) with respect to γ , the PDF of γ can be expressed as (13) shown at the bottom of this page. Similarly, when $\xi_{\text{mod}}^2 \rightarrow \infty$, (13) is reduced to the PDF expression without pointing errors.

Proof: See Appendix B.

B. Variable-Gain Relaying

1) Cumulative Distribution Function:

a) *Exact Analysis*: Since the SINR statistic in (10) is mathematically intractable, we approximate it as $\gamma = \min(\gamma_1^{\text{eff}}, \gamma_2)$ as in [21], [42], [53], which is also the SINR statistics for the DF relaying system. Therefore, the approximate performance curves of the variable-gain AF relaying system are equivalent to those of the DF relaying system. The CDF of γ of the considered dual-hop RF/FSO variable-gain relaying system can be expressed as

$$F_\gamma(\gamma) = F_{\gamma_1^{\text{eff}}}(\gamma) + F_{\gamma_2}(\gamma) - F_{\gamma_1^{\text{eff}}}(\gamma)F_{\gamma_2}(\gamma), \quad (14)$$

where

$$F_{\gamma_1^{\text{eff}}}(\gamma) = 1 - \sum_{i=0}^M \sum_{\ell=0}^{M_X} \sum_{j=0}^{m_i-1} \frac{C_i C_{X,\ell} \gamma^j e^{-\frac{\gamma}{\Omega_i}}}{\Gamma(j+1) \Omega_{X,\ell}^{m_{X,\ell}} \Omega_i^j} \times U\left(m_{X,\ell}, m_{X,\ell} + 1 + j, \frac{1}{\Omega_{X,\ell}} + \frac{\gamma}{\Omega_i}\right), \quad (15)$$

where $U(a, b, z)$ is the confluent hypergeometric function of second kind ((9.211.4) in [47]).

Proof: See Appendix C.

b) *Asymptotic Analysis*: Similarly, for infinite $\bar{\gamma}_1$ and μ_r , the asymptotic CDF can be obtained as (16) shown at the bottom of the next page. From the asymptotic result, we can see that the diversity order is $G_d = 0$.

2) *Probability Density Function*: By differentiating (14) with respect to γ and using (07.34.20.0001.01) in [54], the PDF of γ can be written as

$$f_\gamma(\gamma) = f_{\gamma_1^{\text{eff}}}(\gamma) + f_{\gamma_2}(\gamma) - f_{\gamma_1^{\text{eff}}}(\gamma)F_{\gamma_2}(\gamma) - F_{\gamma_1^{\text{eff}}}(\gamma)f_{\gamma_2}(\gamma), \quad (17)$$

where

$$f_{\gamma_1^{\text{eff}}}(\gamma) = \sum_{i=0}^M \sum_{\ell=0}^{M_X} \sum_{j=0}^{m_i-1} \sum_{s=0}^j \frac{C_i C_{X,\ell} \Omega_{X,\ell}^s \gamma^j e^{-\frac{\gamma}{\Omega_i}}}{\Gamma(m_{X,\ell}) \Gamma(s+1) \Gamma(j-s+1) \Omega_i^j}$$

$$F_\gamma(\gamma) = 1 - \frac{\xi_{\text{mod}}^2}{r\Gamma(a)\Gamma(b)} \sum_{i=0}^M \sum_{\ell=0}^{M_X} \sum_{j=0}^{m_i-1} \sum_{k=0}^j \sum_{s=0}^{j-k} \binom{j}{k} \frac{C_i C_{X,\ell} \Gamma(j-k+1) \Omega_{X,\ell}^s \gamma^{j-k} e^{-\frac{\gamma}{\Omega_i}}}{\Gamma(m_{X,\ell}) \Gamma(j+1) \Gamma(s+1) \Gamma(j-k-s+1) \Omega_i^{j-k}} \times \text{H}_{2,3}^{3,1} \left[\frac{a\varphi C^{\frac{1}{r}} \gamma^{\frac{1}{r}}}{(b-1)\mu_r^{\frac{1}{r}} \Omega_i^{\frac{1}{r}}} \middle| (1-b, 1), (\xi_{\text{mod}}^2 + 1, 1) \right] \text{G}_{1,1}^{1,1} \left[\frac{\Omega_{X,\ell} \gamma}{\Omega_i} \middle| 1 - m_{X,\ell} - s \right]. \quad (11)$$

$$F_\gamma(\gamma) \approx 1 - \frac{\xi_{\text{mod}}^2}{r\Gamma(a)\Gamma(b)} \sum_{i=0}^M \sum_{\ell=0}^{M_X} \sum_{j=0}^{m_i-1} \sum_{k=0}^j \sum_{s=0}^{j-k} \binom{j}{k} \frac{C_i C_{X,\ell} \Gamma(j-k+1) \Gamma(m_{X,\ell} + s) \Omega_{X,\ell}^s \gamma^{j-k}}{\Gamma(m_{X,\ell}) \Gamma(j+1) \Gamma(s+1) \Gamma(j-k-s+1)} \times \frac{\left(1 - \frac{\gamma}{\Omega_i}\right) (\Omega_i + \Omega_{X,\ell} \gamma)^{-m_{X,\ell} - s}}{\Omega_i^{j-k-m_{X,\ell} - s}} \left\{ \Gamma(a - \xi_{\text{mod}}^2) \Gamma\left(k - \frac{\xi_{\text{mod}}^2}{r}\right) \Gamma(b + \xi_{\text{mod}}^2) \left[\frac{a\varphi C^{\frac{1}{r}} \gamma^{\frac{1}{r}}}{(b-1)\mu_r^{\frac{1}{r}} \Omega_i^{\frac{1}{r}}} \right]^{\xi_{\text{mod}}^2} + \frac{\Gamma\left(k - \frac{a}{r}\right) \Gamma(a+b)}{(\xi_{\text{mod}}^2 - a)} \left[\frac{a\varphi C^{\frac{1}{r}} \gamma^{\frac{1}{r}}}{(b-1)\mu_r^{\frac{1}{r}} \Omega_i^{\frac{1}{r}}} \right]^a + \frac{r\Gamma(a-rk) \Gamma(b+rk)}{(\xi_{\text{mod}}^2 - rk)} \left[\frac{a\varphi C^{\frac{1}{r}} \gamma^{\frac{1}{r}}}{(b-1)\mu_r^{\frac{1}{r}} \Omega_i^{\frac{1}{r}}} \right]^{rk} \right\}. \quad (12)$$

$$f_\gamma(\gamma) = \frac{\xi_{\text{mod}}^2}{r\Gamma(a)\Gamma(b)} \sum_{i=0}^M \sum_{\ell=0}^{M_X} \sum_{j=0}^{m_i-1} \sum_{k=0}^j \sum_{s=0}^{j-k} \binom{j}{k} \frac{C_i C_{X,\ell} \Gamma(j-k+1) \Omega_{X,\ell}^s}{\Gamma(m_{X,\ell}) \Gamma(j+1) \Gamma(s+1) \Gamma(j-k-s+1) \Omega_i^{j-k}} \times \left\{ \gamma^{j-k} e^{-\frac{\gamma}{\Omega_i}} \left\{ \left(-\frac{j-k}{\gamma} + \frac{1}{\Omega_i} \right) \text{G}_{1,1}^{1,1} \left[\frac{\Omega_{X,\ell} \gamma}{\Omega_i} \middle| 1 - m_{X,\ell} - s \right] - \frac{1}{\gamma} \text{G}_{2,2}^{1,2} \left[\frac{\Omega_{X,\ell} \gamma}{\Omega_i} \middle| 0, 1 - m_{X,\ell} - s \right] \right\} \right. \\ \times \text{H}_{2,3}^{3,1} \left[\frac{a\varphi C^{\frac{1}{r}} \gamma^{\frac{1}{r}}}{(b-1)\mu_r^{\frac{1}{r}} \Omega_i^{\frac{1}{r}}} \middle| (1-b, 1), (\xi_{\text{mod}}^2 + 1, 1) \right] + \frac{1}{r} \gamma^{j-k-1} e^{-\frac{\gamma}{\Omega_i}} \text{G}_{1,1}^{1,1} \left[\frac{\Omega_{X,\ell} \gamma}{\Omega_i} \middle| 1 - m_{X,\ell} - s \right] \\ \left. \times \text{H}_{3,4}^{4,1} \left[\frac{a\varphi C^{\frac{1}{r}} \gamma^{\frac{1}{r}}}{(b-1)\mu_r^{\frac{1}{r}} \Omega_i^{\frac{1}{r}}} \middle| (1-b, 1), (\xi_{\text{mod}}^2 + 1, 1), (0, 1) \right] \right\}. \quad (13)$$

$$\times \left\{ \left(\frac{1}{\Omega_i} - \frac{j}{\gamma} \right) G_{1,1}^{1,1} \left[\frac{\Omega_{X,\ell}\gamma}{\Omega_i} \middle| \begin{matrix} 1 - m_{X,\ell} - s \\ 0 \end{matrix} \right] - \frac{1}{\gamma} G_{2,2}^{1,2} \left[\frac{\Omega_{X,\ell}\gamma}{\Omega_i} \middle| \begin{matrix} 0, 1 - m_{X,\ell} - s \\ 0, 1 \end{matrix} \right] \right\}. \quad (18)$$

IV. END-TO-END PERFORMANCE METRICS

In this section, the average BER and ergodic capacity are analyzed for both fixed-gain relaying and variable-gain scenarios.

A. Fixed-Gain Relaying

a) *Exact Analysis*: The average BER for different binary modulations is written as [55]

$$\bar{P}_e = \frac{q^p}{2\Gamma(p)} \int_0^\infty \exp(-q\gamma) \gamma^{p-1} F_\gamma(\gamma) d\gamma, \quad (19)$$

where the parameters p and q represent different modulation schemes, as shown in Table I of [9]. Inserting (11) into (19), \bar{P}_e can be derived as (20) shown at the bottom of this page. Similarly, when $\xi_{\text{mod}}^2 \rightarrow \infty$, \bar{P}_e without pointing errors can be obtained.

Proof: See Appendix D.

b) *Asymptotic Analysis*: At high SNRs, inserting (12) into (19) and using (07.34.21.0012.01) in [54], the asymptotic BER

is derived as (21) shown at the bottom of this page. where $\Delta_1 = \frac{a\varphi C^{\frac{1}{r}}}{(b-1)\mu_r^{\frac{1}{r}} \Omega_i^{\frac{1}{r}}}$ and $\Delta_2 = \frac{\Omega_i}{q\Omega_i+1}$.

2) *Ergodic Capacity*: From [17], the ergodic capacity can be computed as

$$\bar{C} = \frac{c}{2 \ln 2} \int_0^\infty \frac{1 - F_\gamma(\gamma)}{1 + c\gamma} d\gamma, \quad (22)$$

where $c = 1$ for HD; and $c = e/(2\pi)$ for DD. Unfortunately, by substituting (11) or (12) into (22), such an integral is extremely complicated. Nevertheless, by performing the change of variables $\gamma = \tan \theta$ and using a N_p -point Gauss Chebyshev Quadrature (GCQ) rule formula ((25.4.39) in [56]), \bar{C} can be easily estimated as

$$\bar{C} \approx \frac{c}{2 \ln 2} \sum_{n=1}^{N_p} w_n \frac{1 - F_\gamma(x_n)}{1 + cx_n}, \quad (23)$$

where the abscissas x_n and the weights w_n are expressed as (22) and (23) in [57], respectively. It is noted that (23) requires only few terms to get a sufficient approximation accuracy.

B. Variable-Gain Relaying

1) Average Bit Error Rate:

$$F_\gamma(\gamma) \approx 1 - \sum_{i=0}^M \sum_{\ell=0}^{M_X} \sum_{j=0}^{m_i-1} \sum_{s=0}^j \frac{C_i C_{X,\ell} \Gamma(m_{X,\ell} + s) \Omega_{X,\ell}^s \gamma^j e^{-\frac{\gamma}{\Omega_i}} (\Omega_i + \Omega_{X,\ell}\gamma)^{-m_{X,\ell}-s}}{\Gamma(m_{X,\ell}) \Gamma(s+1) \Gamma(j-s+1) \Omega_i^{j-m_{X,\ell}-s}} + \frac{\xi_{\text{mod}}^2 \Gamma(a+b)}{\Gamma(a+1) \Gamma(b) (\xi_{\text{mod}}^2 - a)} \left[\frac{a\varphi\gamma^{\frac{1}{r}}}{(b-1)\mu_r^{\frac{1}{r}}} \right]^a + \frac{\Gamma(a - \xi_{\text{mod}}^2) \Gamma(b + \xi_{\text{mod}}^2)}{\Gamma(a)\Gamma(b)} \left[\frac{a\varphi\gamma^{\frac{1}{r}}}{(b-1)\mu_r^{\frac{1}{r}}} \right]^{\xi_{\text{mod}}^2}. \quad (16)$$

$$\bar{P}_e = \frac{1}{2} - \frac{q^p \xi_{\text{mod}}^2}{2r\Gamma(a)\Gamma(b)\Gamma(p)} \sum_{i=0}^M \sum_{\ell=0}^{M_X} \sum_{j=0}^{m_i-1} \sum_{k=0}^j \sum_{s=0}^{j-k} \binom{j}{k} \times \frac{C_i C_{X,\ell} \Gamma(j-k+1) \Omega_i^p \Omega_{X,\ell}^s}{\Gamma(m_{X,\ell}) \Gamma(j+1) \Gamma(s+1) \Gamma(j-k-s+1) (q\Omega_i+1)^{j+p-k}} \times \mathbf{H}_{1,0;2,3;1,1}^{0,1;3,1;1,1} \left[\frac{a\varphi C^{\frac{1}{r}}}{(b-1)\mu_r^{\frac{1}{r}} (q\Omega_i+1)^{\frac{1}{r}}}, \frac{\Omega_{X,\ell}}{q\Omega_i+1} \middle| \begin{matrix} (1-j-p+k, \frac{1}{r}, 1) : (1-b, 1), (\xi_{\text{mod}}^2+1, 1) : (1-m_{X,\ell}-s, 1) \\ - : (a, 1), (\xi_{\text{mod}}^2, 1), (k, \frac{1}{r}) : (0, 1) \end{matrix} \right]. \quad (20)$$

$$\bar{P}_e \approx \frac{1}{2} - \frac{q^p \xi_{\text{mod}}^2}{2r\Gamma(a)\Gamma(b)\Gamma(p)} \sum_{i=0}^M \sum_{\ell=0}^{M_X} \sum_{j=0}^{m_i-1} \sum_{k=0}^j \sum_{s=0}^{j-k} \binom{j}{k} \frac{C_i C_{X,\ell} \Gamma(j-k+1) \Omega_{X,\ell}^s}{\Gamma(m_{X,\ell}) \Gamma(j+1) \Gamma(s+1) \Gamma(j-k-s+1) \Omega_i^{j-k}} \times \left\{ \frac{\Gamma(k - \frac{a}{r}) \Gamma(a+b)}{(\xi_{\text{mod}}^2 - a) \Delta_1^{-a} \Delta_2^{-\frac{a}{r}-j-p+k}} \mathbf{H}_{2,1}^{1,2} \left[\frac{\Omega_{X,\ell}}{q\Omega_i+1} \middle| \begin{matrix} (1-m_{X,\ell}-s, 1), (1-\frac{a}{r}-j-p+k, 1) \\ (0, 1) \end{matrix} \right] + \frac{\Gamma(a - \xi_{\text{mod}}^2) \Gamma(k - \frac{\xi_{\text{mod}}^2}{r}) \Gamma(b + \xi_{\text{mod}}^2)}{\Delta_1^{-\xi_{\text{mod}}^2} \Delta_2^{-\frac{\xi_{\text{mod}}^2}{r}-j-p+k}} \mathbf{H}_{2,1}^{1,2} \left[\frac{\Omega_{X,\ell}}{q\Omega_i+1} \middle| \begin{matrix} (1-m_{X,\ell}-s, 1), (1-\frac{\xi_{\text{mod}}^2}{r}-j-p+k, 1) \\ (0, 1) \end{matrix} \right] + \frac{r\Gamma(a-rk) \Gamma(b+rk)}{(\xi_{\text{mod}}^2 - rk) \Delta_1^{-rk} \Delta_2^{-j-p}} \mathbf{H}_{2,1}^{1,2} \left[\frac{\Omega_{X,\ell}}{q\Omega_i+1} \middle| \begin{matrix} (1-m_{X,\ell}-s, 1), (1-j-p, 1) \\ (0, 1) \end{matrix} \right] \right\}, \quad (21)$$

a) *Exact Analysis:* Substituting (14) into (19), and using (8.4.3.1) in [49], (07.34.21.0012.01) in [54], and (2.3) in [58], the average BER is given as (24) shown at the bottom of this page. Similarly, when $\xi_{\text{mod}}^2 \rightarrow \infty$, \bar{P}_e without pointing errors can be obtained.

b) *Asymptotic Analysis:* At high SNRs, substituting (16) into (19) and using (07.34.21.0012.01) in [54], the asymptotic BER is derived as (25) shown at the bottom of this page.

Notice that at high SNRs, the interference-limited RF link becomes dominant, so \bar{P}_e asymptotically approaches an identical fixed error floor value for both fixed-gain and variable-gain relaying scenarios. From the asymptotic expressions, the error floor value is approximately equal to first two terms of (25) (first line of (25)).

2) *Ergodic Capacity:* Utilizing the same method similar to the fixed-gain relaying scenario, the ergodic capacity can be obtained as

$$\bar{C} \approx \frac{c}{2 \ln 2} \sum_{n=1}^{N_p} w_n \frac{1 - F_{\gamma}(x_n)}{1 + cx_n}. \quad (26)$$

V. NUMERICAL RESULTS

Using the analysis presented in Section IV, numerical results compared with Monte Carlo (MC) simulations are presented for both fixed-gain and variable-gain relaying scenarios. Without loss of generality, we set $\bar{\gamma}_1 = \bar{\gamma}_2$. Unless otherwise stated, the following parameters are considered. For the RF channel, the fading parameters set as follows: $\kappa = 4$, $\mu = 5$, $m = 8$, and $N = 2$. As described in [41], we also set the interference power to be proportional to the transmitted power ($P_s/P_i = 15$ dB). For interference parameters, we set $\mu_I = 1$, $\kappa_I \rightarrow 0$, and $m_I \rightarrow \infty$, in which the κ - μ shadowed distribution is reduced to the Rayleigh distribution. For the FSO channel, the turbulence parameters are listed as: moderate turbulence ($a =$

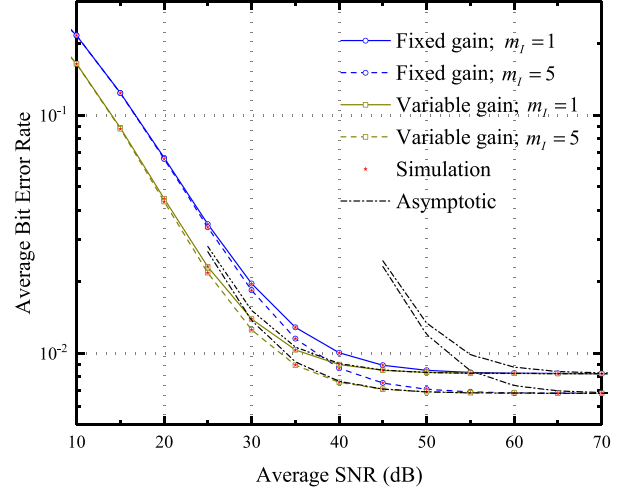


Fig. 2. Average BER with DBPSK modulation versus average SNR with different shadowing values m_I under moderate turbulence condition.

1.83, $b = 3.94$), strong turbulence ($a = 1.43$, $b = 3.53$). For such values, the corresponding Rytov variances are $\beta_0^2 = 1.61$ and $\beta_0^2 = 6.44$, respectively. The strong pointing errors are set to $\xi_{\text{mod}} = 1.26$ for all BER curves and $\xi_{\text{mod}} = 0.84$ for all ergodic capacity curves, respectively.

In Fig. 2, we plot the average BER versus average SNR with fixed values of $\xi_{\text{mod}} = 5.03$, $\kappa_I = 4$, $\mu_I = 5$, $N = 5$ and different values of m_I for both fixed-gain and variable-gain relaying scenarios. The analytical results based on (20) and (24) coincide with the MC simulations, indicating the accuracy of our derivation. At high SNRs and under both gain scenarios, it can be noticed that increasing m_I improves the BER performance as the interference links become more static with higher values of m_I . As expected, the BER performance deteriorates significantly

$$\begin{aligned} \bar{P}_e &= \frac{1}{2} - \frac{q^p}{2\Gamma(p)} \sum_{i=0}^M \sum_{\ell=0}^{M_X} \sum_{j=0}^{m_i-1} \sum_{s=0}^j \frac{C_i C_{X,\ell} \Omega_i^p \Omega_{X,\ell}^s}{\Gamma(m_{X,\ell}) \Gamma(s+1) \Gamma(j-s+1) (q\Omega_i + 1)^{j+p}} \\ &\times \mathbf{H}_{2,1}^{1,2} \left[\frac{\Omega_{X,\ell}}{q\Omega_i + 1} \middle| \begin{matrix} (1 - m_{X,\ell} - s, 1), (1 - j - p, 1) \\ (0, 1) \end{matrix} \right] \\ &+ \frac{q^p \xi_{\text{mod}}^2}{2\Gamma(a)\Gamma(b)\Gamma(p)} \sum_{i=0}^M \sum_{\ell=0}^{M_X} \sum_{j=0}^{m_i-1} \sum_{s=0}^j \frac{C_i C_{X,\ell} \Omega_i^p \Omega_{X,\ell}^s}{\Gamma(m_{X,\ell}) \Gamma(s+1) \Gamma(j-s+1) (q\Omega_i + 1)^{j+p}} \\ &\times \mathbf{H}_{1,0:3,3:1,1}^{0,1:2,2:1,1} \left[\frac{a\varphi \Omega_i^{\frac{1}{r}}}{(b-1)\mu_r^{\frac{1}{r}} (q\Omega_i + 1)^{\frac{1}{r}}}, \frac{\Omega_{X,\ell}}{q\Omega_i + 1} \middle| \begin{matrix} (1 - j - p, \frac{1}{r}, 1) : (1 - b, 1), (1, 1), (\xi_{\text{mod}}^2 + 1, 1) : (1 - m_{X,\ell} - s, 1) \\ - : (a, 1), (\xi_{\text{mod}}^2, 1), (0, 1) : (0, 1) \end{matrix} \right]. \end{aligned} \quad (24)$$

$$\begin{aligned} \bar{P}_e &\approx \frac{1}{2} - \frac{q^p}{2\Gamma(p)} \sum_{i=0}^M \sum_{\ell=0}^{M_X} \sum_{j=0}^{m_i-1} \sum_{s=0}^j \frac{C_i C_{X,\ell} \Omega_i^p \Omega_{X,\ell}^s (q\Omega_i + 1)^{-j-p}}{\Gamma(m_{X,\ell}) \Gamma(s+1) \Gamma(j-s+1)} \mathbf{H}_{2,1}^{1,2} \left[\frac{\Omega_{X,\ell}}{q\Omega_i + 1} \middle| \begin{matrix} (1 - m_{X,\ell} - s, 1), (1 - j - p, 1) \\ (0, 1) \end{matrix} \right] \\ &+ \frac{\xi_{\text{mod}}^2 \Gamma(a+b)\Gamma(\frac{a}{r}+p)}{2\Gamma(a+1)\Gamma(b)\Gamma(p)(\xi_{\text{mod}}^2 - a)} \left[\frac{a\varphi}{(b-1)q^{\frac{1}{r}}\mu_r^{\frac{1}{r}}} \right]^a + \frac{\Gamma(a - \xi_{\text{mod}}^2) \Gamma(b + \xi_{\text{mod}}^2) \Gamma(\frac{\xi_{\text{mod}}^2}{r} + p)}{2\Gamma(a)\Gamma(b)\Gamma(p)} \left[\frac{a\varphi}{(b-1)q^{\frac{1}{r}}\mu_r^{\frac{1}{r}}} \right]^{\xi_{\text{mod}}^2}. \end{aligned} \quad (25)$$

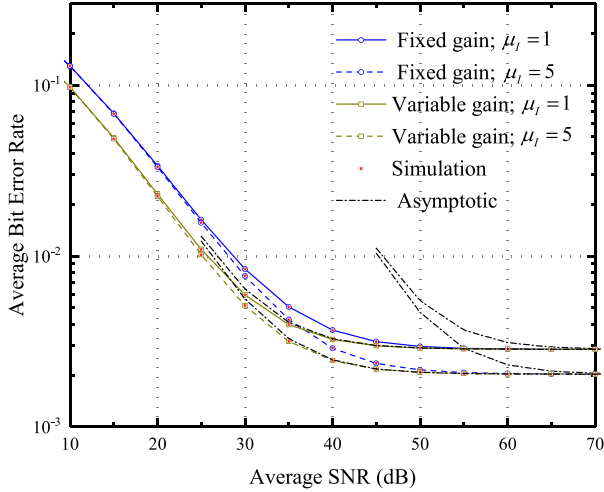


Fig. 3. Average BER with BPSK modulation versus average SNR with different cluster numbers μ_I under moderate turbulence condition.

in the presence CCIs. Moreover, at high SNRs for both gain scenarios, we observe that BER floors happen in the presence of CCIs and do not appear in the absence of CCIs. In the operating region of an average SNR between 20 and 30 dB, the slopes of the BER curves for fixed-gain relaying scenario are about 3.00 and 3.13 for $m_I = 1$ and $m_I = 5$, respectively; the slopes of the BER curves for variable-gain relaying scenario are about 2.87 and 3.06 for $m_I = 1$ and $m_I = 5$, respectively. Also, we observe that the asymptotic expressions in (21) and (25) match well with the exact results at high SNRs.

In Fig. 3, we plot the average BER versus average SNR with fixed values of $\xi_{\text{mod}} = 5.03$, $\kappa_I = 0.1$, $m_I = 8$, $N = 5$ and different values of μ_I for both fixed-gain and variable-gain relaying scenarios. It can be noticed that the impact of cluster numbers of the interference links on the BER performance depends on the SNR. For example, at large SNR values and under both gain scenarios, less severe fading interference links (i.e., large μ_I) may lead to a better BER performance, otherwise, more severe fading interference links (i.e., small μ_I) may result in a worse BER performance. In addition, at high SNRs for both gain scenarios, we observe that BER floors happen in the presence of CCIs and do not appear in the absence of CCIs. In the operating region of an average SNR between 20 and 30 dB, the slopes of the BER curves for fixed-gain relaying scenario are about 3.42 and 3.61 for $\mu_I = 1$ and $\mu_I = 5$, respectively; the slopes of the BER curves for variable-gain relaying scenario are about 3.36 and 3.63 for $\mu_I = 1$ and $\mu_I = 5$, respectively.

In Fig. 4, we plot the average BER versus average SNR for both fixed-gain and variable-gain relaying scenarios with CCIs ($P_s/P_i = 10$ dB) under moderate and strong turbulence conditions. It can be seen that increasing the intensity of turbulence results in poor system performance for both gain scenarios. For comparison, the BER performance of the considered system without CCIs is also provided. As expected, the BER performance deteriorates significantly in the presence CCIs compared to no CCIs case. Moreover, at high SNRs for both gain

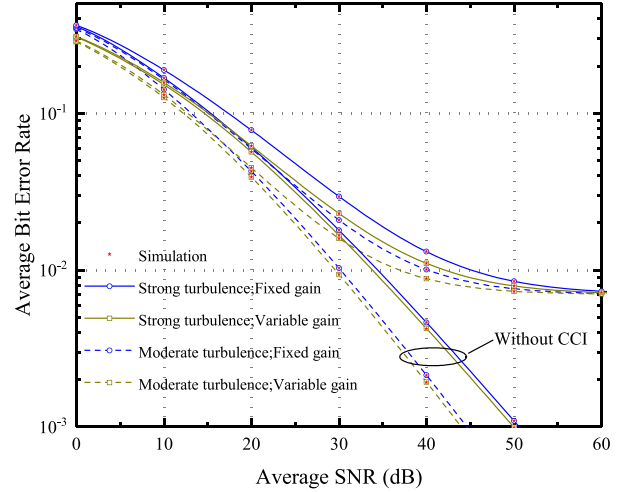


Fig. 4. Average BER with BPSK modulation versus average SNR under moderate and strong turbulence conditions with and without CCI.

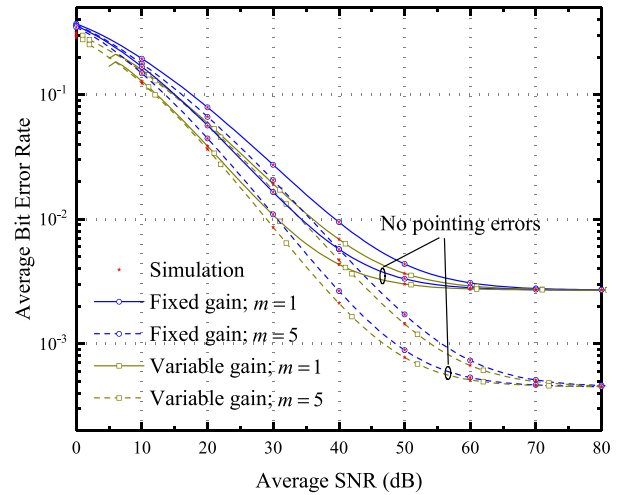


Fig. 5. Average BER with BPSK modulation versus average SNR with various shadowing values m under strong turbulence condition.

scenarios, we observe that BER floors happen in the presence of CCIs and do not appear in the absence of CCIs.

In Fig. 5, we plot the average BER versus average SNR for both fixed-gain and variable-gain relaying scenarios with different values of m . We observe that BER performance deteriorates with decreasing value of m . Expectedly, pointing errors reduce the system BER performance for a wide range of SNRs. Moreover, at high SNRs for both gain scenarios, we observe that BER floors happen and the BER performance converges to the same values for the same values of m , meaning that increasing the average SNR does not improve the system performance. This is because that at high SNRs, the interference-limited RF link becomes dominant considering that the interference power is scaled with the transmitted power. In addition, the occurrence of BER floors for large values of m may require a higher average SNR than that for small values of m . In Fig. 6, we plot the average BER versus average SNR for both fixed-gain and variable-gain

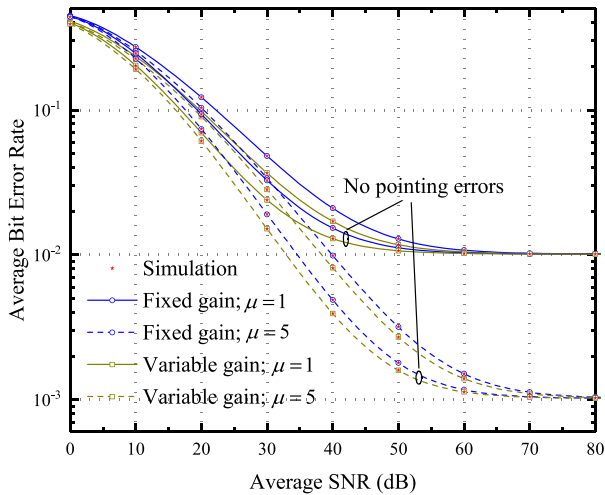


Fig. 6. Average BER with DBPSK modulation versus average SNR with different cluster numbers μ under strong turbulence condition.

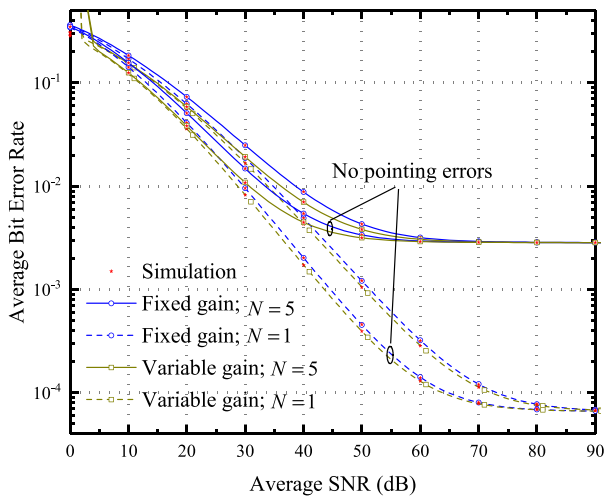


Fig. 7. Average BER with BPSK modulation versus average SNR with different number of interferers under strong turbulence condition.

relaying scenarios with different values of μ . We also draw some conclusions similar to Fig. 5.

In Fig. 7, we plot the average BER versus average SNR for both fixed-gain and variable-gain relaying scenarios with different values of N . As expected, increasing the number of interferers results in higher BER for both gain scenarios. From this figure, we can observe that the pointing error degrades the system BER performance for a wide range of SNRs. In addition, at high SNRs, we also observe that BER floors happen for both gain scenarios, and higher average SNR may be required for the occurrence of BER floors for small values of N . This is mainly due to the effect of CCIs.

In Fig. 8, we plot the ergodic capacity versus average SNR for both fixed-gain and variable-gain relaying scenarios with CCIs ($P_s/P_i = 10$ dB) under moderate and strong turbulence conditions. It can be seen that increasing the intensity of turbulence results in poor system performance for both gain

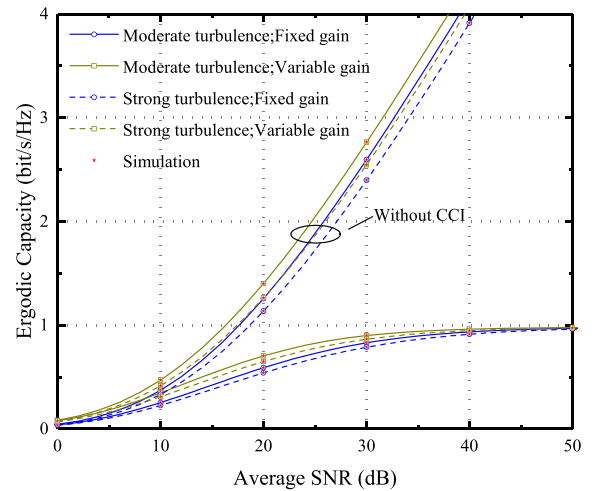


Fig. 8. Ergodic capacity versus average SNR under moderate and strong turbulence conditions with and without CCI.

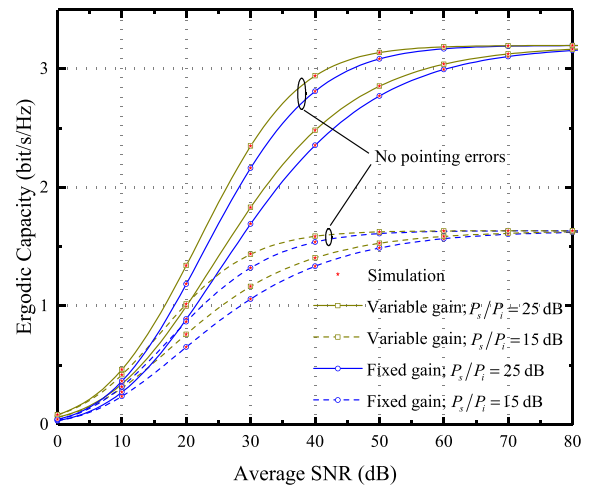


Fig. 9. Ergodic capacity versus average SNR with different interference power under strong turbulence condition.

scenarios. In addition, for the evaluation of the ergodic capacity in (23) and (26), $N_p = 60$ was used for enough accuracy. From this figure, we can observe that the numerical results match well with the MC simulations. For comparison, we also provide the ergodic capacity performance of the considered system in the absence of CCIs. As expected, the ergodic capacity performance deteriorates significantly in the presence of CCIs compared to no CCIs case. Moreover, at high SNRs for both gain scenarios, we observe that capacity ceilings happen in the presence of CCIs and do not appear in the absence of CCIs.

In Fig. 9, we plot the ergodic capacity versus average SNR for both fixed-gain and variable-gain relaying scenarios with different interference power. As expected, with an increase of interference power, the ergodic capacity decreases for both gain scenarios. It can be observed that the pointing error reduces the ergodic capacity for a wide range of SNRs. In addition, at high SNRs, capacity ceilings appear for both gain scenarios, and the occurrence of capacity ceilings for lower interference

power may require a higher average SNR than that for larger interference power. Furthermore, as the average SNR increases, the ergodic capacity first increases, then stabilizes and converges to the same values for the same interference power, because the interference-limited RF link dominates the system performance at high SNRs.

In addition, from Figs. 2, 3, 4, 5, 6, 7, 8, and 9, we note that in the presence of CCIs, at high SNRs, BER floors and capacity ceilings happen, and the BER and capacity performance will converge to the same values for the same RF link parameters. This is because that at high SNRs, the interference-limited RF link becomes dominant considering that the interference power is set to be proportional to the transmitted power. This also shows that diversity order of zero is obtained. We also find the variable-gain relaying scenario performs better than the fixed-gain relaying scenario for a wide range of SNRs when the RF link and the FSO link have the same average SNR. This phenomenon can be explained as follows. The relay node R amplifies the RF signal received from the first-hop link in different ways. Specifically, for the variable-gain relaying scenario, the scaling gain is adaptively changed according to the instantaneous channel state information (CSI) of the first-hop link in order to maintain a constant output power; in contrast, for the fixed-gain relaying scenario, the scaling gain is only dependent on the statistical CSI of the first-hop link. Therefore, the variable-gain relaying system always outperforms the fixed-gain relaying system at the expense of the processing complexity at the relay node R.

VI. CONCLUSION

We have investigated the performance of dual-hop mixed RF/FSO relaying systems under both fixed-gain and variable-gain relaying scenarios with CCIs at the relay node. The RF and FSO links are modeled by the κ - μ shadowed distribution and the Fisher-Snedecor \mathcal{F} distribution with pointing errors, respectively. We derived new closed-form expressions and asymptotic expressions for the CDF and average BER of the considered system. We also presented efficient numerical expressions for the ergodic capacity by using GCQ rule formula. We have verified the analytical results through the MC simulations. These new results allow us to investigate the impacts of number of interferers, interference power, cluster numbers, and shadowing parameter, atmospheric turbulence, pointing errors, and different forward protocols on the considered system's performance. In addition, we found that BER floors and capacity ceilings appear for the interference-limited case and don't appear for the interference-free case at high SNRs. We also found that the

variable-gain relaying scenario outperforms fixed-gain relaying scenario for a wide range of SNRs in our system. This work provides closed-form and generalized models for the design and analysis of dual-hop mixed RF/FSO relaying systems when both CCIs and pointing errors are present.

DISCLOSURES

The authors declare no conflicts of interest.

DATA AVAILABILITY

Data underlying the results presented in this paper were generated using the equations herein.

APPENDIX A DERIVATION OF (11)

The CDF of γ can be expressed as

$$\begin{aligned} F_\gamma(\gamma) &= \Pr \left[\frac{\gamma_1 \gamma_2}{\gamma_2 \gamma_I + \gamma_2 + C} < \gamma | \gamma_2 \right] \\ &= \int_0^\infty \int_0^\infty \Pr \left[\gamma_1 < \gamma \left(\gamma_I + 1 + \frac{C}{\gamma_2} \right) \right] \\ &\quad \times f_{\gamma_2}(\gamma_2) f_{\gamma_I}(\gamma_I) d\gamma_2 d\gamma_I. \end{aligned} \quad (\text{A.1})$$

Inserting (4), (5), and (7) into (A.1), we get (A.2) shown at the bottom of this page.

Finally, using (9.211.4) in [47] and (07.34.21.0012.01) in [54], $F_\gamma(\gamma)$ can be derived as (11).

APPENDIX B DERIVATION OF (13).

To facilitate the derivation of the PDF of γ , we set

$$\begin{aligned} g(\gamma) &= \gamma^{j-k} e^{-\frac{\gamma}{\Omega_i}} G_{1,1}^{1,1} \left[\frac{\Omega_{X,\ell} \gamma}{\Omega_i} \middle| \begin{matrix} 1 - m_{X,\ell} - s \\ 0 \end{matrix} \right] \\ &\quad \times H_{2,3}^{3,1} \left[\frac{a \varphi C^{\frac{1}{r}} \gamma^{\frac{1}{r}}}{(b-1) \mu_r^{\frac{1}{r}} \Omega_i^{\frac{1}{r}}} \middle| \begin{matrix} (1-b, 1), (\xi_{\text{mod}}^2 + 1, 1) \\ (a, 1), (\xi_{\text{mod}}^2, 1), (k, \frac{1}{r}) \end{matrix} \right]. \end{aligned} \quad (\text{B.1})$$

Differentiating $g(\gamma)$ with respect to γ , we obtain

$$\begin{aligned} \frac{dg(\gamma)}{d\gamma} &= \left\{ \gamma^{j-k} e^{-\frac{\gamma}{\Omega_i}} G_{1,1}^{1,1} \left[\frac{\Omega_{X,\ell} \gamma}{\Omega_i} \middle| \begin{matrix} 1 - m_{X,\ell} - s \\ 0 \end{matrix} \right] \right\}' \\ &\quad \times H_{2,3}^{3,1} \left[\frac{a \varphi C^{\frac{1}{r}} \gamma^{\frac{1}{r}}}{(b-1) \mu_r^{\frac{1}{r}} \Omega_i^{\frac{1}{r}}} \middle| \begin{matrix} (1-b, 1), (\xi_{\text{mod}}^2 + 1, 1) \\ (a, 1), (\xi_{\text{mod}}^2, 1), (k, \frac{1}{r}) \end{matrix} \right] \end{aligned}$$

$$\begin{aligned} F_\gamma(\gamma) &= 1 - \frac{\xi_{\text{mod}}^2}{r \Gamma(a) \Gamma(b)} \sum_{i=0}^M \sum_{\ell=0}^{M_X} \sum_{j=0}^{m_i-1} \sum_{k=0}^j \binom{j}{k} \frac{C_i C_{X,\ell} C^k \gamma^j e^{-\frac{\gamma}{\Omega_i}}}{\Gamma(m_{X,\ell}) \Gamma(j+1) \Omega_{X,\ell}^{m_{X,\ell}} \Omega_i^j} \\ &\quad \times \int_0^\infty \gamma_2^{-k-1} G_{1,0}^{0,1} \left[\frac{\Omega_i \gamma_2}{\gamma C} \middle| \begin{matrix} 1 \\ - \end{matrix} \right] G_{2,2}^{2,1} \left[\frac{a \varphi \gamma_2^{\frac{1}{r}}}{(b-1) \mu_r^{\frac{1}{r}}} \middle| \begin{matrix} 1-b, \xi_{\text{mod}}^2 + 1 \\ a, \xi_{\text{mod}}^2 \end{matrix} \right] d\gamma_2 \times \int_0^\infty \gamma_I^{m_{X,\ell}-1} (\gamma_I + 1)^{j-k} e^{-\left(\frac{\gamma}{\Omega_i} + \frac{1}{\Omega_{X,\ell}}\right) \gamma_I} d\gamma_I. \end{aligned} \quad (\text{A.2})$$

$$\begin{aligned} \bar{P}_e &= \frac{1}{2} - \frac{q^p \xi_{\text{mod}}^2}{2r\Gamma(a)\Gamma(b)\Gamma(p)} \sum_{i=0}^M \sum_{\ell=0}^{M_X} \sum_{j=0}^{m_i-1} \sum_{k=0}^j \sum_{s=0}^{j-k} \binom{j}{k} \\ &\times \frac{C_i C_{X,\ell} \Gamma(j-k+1) \Omega_{X,\ell}^s}{\Gamma(m_{X,\ell}) \Gamma(j+1) \Gamma(s+1) \Gamma(j-k-s+1) \Omega_i^{j-k}} \int_0^\infty \gamma^{p+j-k-1} G_{0,1}^{1,0} \left[\left(q + \frac{1}{\Omega_i} \right) \gamma \middle| - \right] \\ &\times H_{2,3}^{3,1} \left[\frac{a \xi_{\text{mod}}^2 C_r^{\frac{1}{r}} \gamma^{\frac{1}{r}}}{(b-1) (\xi_{\text{mod}}^2 + 1) \mu_r^{\frac{1}{r}} \Omega_i^{\frac{1}{r}}} \middle| (a, 1), (\xi_{\text{mod}}^2 + 1), (k, \frac{1}{r}) \right] G_{1,1}^{1,1} \left[\frac{\Omega_{X,\ell} \gamma}{\Omega_i} \middle| 1 - m_{X,\ell} - s \right] d\gamma. \quad (\text{D.1}) \end{aligned}$$

$$\begin{aligned} &+ \gamma^{j-k} e^{-\frac{\gamma}{\Omega_i}} G_{1,1}^{1,1} \left[\frac{\Omega_{X,\ell} \gamma}{\Omega_i} \middle| 1 - m_{X,\ell} - s \right] \\ &\times \left\{ H_{2,3}^{3,1} \left[\frac{a \varphi C_r^{\frac{1}{r}} \gamma^{\frac{1}{r}}}{(b-1) \mu_r^{\frac{1}{r}} \Omega_i^{\frac{1}{r}}} \middle| (a, 1), (\xi_{\text{mod}}^2 + 1), (k, \frac{1}{r}) \right] \right\}'. \quad (\text{B.2}) \end{aligned}$$

Finally, using (1.1.1) in [51] and (07.34.20.0001.01) in [54], and employing the differential form of the product rule, $f_\gamma(\gamma)$ can be expressed as (13).

APPENDIX C DERIVATION OF (15)

The CDF of γ_1^{eff} can be written as

$$\begin{aligned} F_{\gamma_1^{\text{eff}}}(\gamma) &= \int_0^\infty \Pr[\gamma_1 < \gamma(\gamma_I + 1) | \gamma_I] f_{\gamma_I}(\gamma_I) d\gamma_I \\ &= \int_0^\infty F_{\gamma_1}[\gamma(\gamma_I + 1)] f_{\gamma_I}(\gamma_I) d\gamma_I. \quad (\text{C.1}) \end{aligned}$$

Inserting (4) and (5) into (C.1), the CDF of γ_1^{eff} can be written as

$$\begin{aligned} F_{\gamma_1^{\text{eff}}}(\gamma) &= 1 - \sum_{i=0}^M \sum_{j=0}^{m_i-1} \sum_{\ell=0}^{M_X} \frac{C_i C_{X,\ell} \gamma^j e^{-\frac{\gamma}{\Omega_i}}}{\Gamma(m_{X,\ell}) \Gamma(j+1) \Omega_{X,\ell}^{m_{X,\ell}} \Omega_i^j} \\ &\times \int_0^\infty (\gamma_I + 1)^j \gamma_I^{m_{X,\ell}-1} e^{-\left(\frac{1}{\Omega_{X,\ell}} + \frac{\gamma}{\Omega_i}\right) \gamma_I} d\gamma_I. \quad (\text{C.2}) \end{aligned}$$

Finally, using (9.211.4) in [47], we arrive at (15).

APPENDIX D DERIVATION OF (20)

Substituting (11) into (19) and then employing (8.4.3.1) in [57], \bar{P}_e can be written as (D.1) shown at the top of this page.

Finally, using (2.9.1) in [51], (1.1.1) in [51], (3.381/4) in [47], and (1.1) in [58], we arrive at (20).

REFERENCES

- [1] S. Biswas, S. Vuppala, J. Xue, and T. Ratnarajah, "On the performance of relay aided millimeter wave networks," *IEEE J. Sel. Topics Signal Process.*, vol. 10, no. 3, pp. 576–588, Apr. 2016.
- [2] E. Balti and M. Guizani, "Mixed RF/FSO cooperative relaying systems with co-channel interference," *IEEE Trans. Commun.*, vol. 66, no. 9, pp. 4014–4027, Sep. 2018.
- [3] I. Trigui, P. D. Diamantoulakis, S. Affes, and G. K. Karagiannidis, "Shadowed FSO/mmWave systems with interference," *IEEE Trans. Commun.*, vol. 67, no. 9, pp. 6256–6267, Sep. 2019.
- [4] L. C. Andrews and R. L. Phillips, *Laser Beam Propagation Through Random Media*. Washington, DC, USA: SPIE Press, 2005.
- [5] H. Wu et al., "Secrecy performance analysis in the FSO communication system considering different eavesdropping scenarios," *Opt. Exp.*, vol. 30, no. 23, pp. 41028–41047, 2022.
- [6] I. S. Ansari, F. Yilmaz, and M.-S. Alouini, "Impact of pointing errors on the performance of mixed RF/FSO dual-hop transmission systems," *IEEE Wireless Commun. Lett.*, vol. 2, no. 3, pp. 351–354, Jun. 2013.
- [7] E. Lee, J. Park, D. Han, and G. Yoon, "Performance analysis of the asymmetric dual-hop relay transmission with mixed RF/FSO links," *IEEE Photon. Technol. Lett.*, vol. 23, no. 21, pp. 1642–1644, Nov. 2011.
- [8] H. Samimi and M. Uysal, "End-to-end performance of mixed RF/FSO transmission systems," *J. Opt. Commun. Netw.*, vol. 5, no. 11, pp. 1139–1144, 2013.
- [9] S. Anees and M. R. Bhatnagar, "Performance of an amplify-and-forward dual-hop asymmetric RF-FSO communication system," *J. Opt. Commun. Netw.*, vol. 7, no. 2, pp. 124–135, 2015.
- [10] J. Zhang, L. Dai, Y. Zhang, and Z. Wang, "Unified performance analysis of mixed radio frequency/free-space optical dual-hop transmission systems," *J. Lightw. Technol.*, vol. 33, no. 11, pp. 2286–2293, Jun. 2015.
- [11] E. Zedini, I. S. Ansari, and M.-S. Alouini, "Performance analysis of mixed Nakagami- m and gamma-gamma dual-hop FSO transmission systems," *IEEE Photon. J.*, vol. 7, no. 1, pp. 1–20, Feb. 2015.
- [12] L. Yang, M. O. Hasna, and I. S. Ansari, "Unified performance analysis for multiuser mixed η - μ and \mathcal{M} -distribution dual-hop RF/FSO systems," *IEEE Trans. Commun.*, vol. 65, no. 8, pp. 3601–3613, Aug. 2017.
- [13] L. Yang, M. O. Hasna, and X. Gao, "Performance of mixed RF/FSO with variable gain over generalized atmospheric turbulence channels," *IEEE J. Sel. Areas Commun.*, vol. 33, no. 9, pp. 1913–1924, Sep. 2015.
- [14] G. Xu and Z. Song, "Performance analysis for mixed κ - μ fading and \mathcal{M} -distribution dual-hop radio frequency/free space optical communication systems," *IEEE Trans. Wireless Commun.*, vol. 20, no. 3, pp. 1517–1528, Mar. 2021.
- [15] P. V. Trinh, T. C. Thang, and A. T. Pham, "Mixed mmwave RF/FSO relaying systems over generalized fading channels with pointing errors," *IEEE Photon. J.*, vol. 9, no. 1, pp. 1–14, Feb. 2017.
- [16] E. Zedini, H. Soury, and M.-S. Alouini, "On the performance analysis of dual-hop mixed FSO/RF systems," *IEEE Trans. Wireless Commun.*, vol. 15, no. 5, pp. 3679–3689, May 2016.
- [17] Q. Sun, Z. Zhang, Y. Zhang, M. López-Benítez, and J. Zhang, "Performance analysis of dual-hop wireless systems over mixed FSO/RF fading channel," *IEEE Access*, vol. 9, pp. 85529–85542, 2021.
- [18] J. Ding, X. Xie, L. Wang, L. Tan, J. Ma, and D. Kang, "Performance of dual-hop FSO/RF systems with fixed-gain relaying over fisher-snedecor 8 and \mathcal{F} and κ - μ shadowed fading channels," *Appl. Opt.*, vol. 61, no. 8, pp. 2079–2088, 2022.
- [19] J. Ding, X. Xie, L. Tan, J. Ma, and D. Kang, "Dual-hop RF/FSO systems over κ - μ shadowed and fisher-snedecor \mathcal{F} fading channels with non-zero boresight pointing errors," *J. Lightw. Technol.*, vol. 40, no. 3, pp. 708–719, Feb. 2022.
- [20] A. Upadhyaya, V. K. Dwivedi, and G. K. Karagiannidis, "On the effect of interference and misalignment error in mixed RF/FSO systems over generalized fading channels," *IEEE Trans. Commun.*, vol. 68, no. 6, pp. 3681–3695, Jun. 2020.
- [21] E. Soleimani-Nasab and M. Uysal, "Generalized performance analysis of mixed RF/FSO cooperative systems," *IEEE Trans. Wireless Commun.*, vol. 15, no. 1, pp. 714–727, Jan. 2016.

- [22] J. M. Garrido-Balsells, A. Jurado-Navas, J. F. Paris, M. Castillo-Vazquez, and A. Puerta-Notario, "Novel formulation of the \mathcal{M} model through the generalized-K distribution for atmospheric optical channels," *Opt. Exp.*, vol. 23, no. 5, pp. 6345–6358, 2015.
- [23] K. P. Peppas, G. C. Alexandropoulos, E. D. Xenos, and A. Maras, "The Fischer-Snedecor \mathcal{F} -distribution model for turbulence-induced fading in free-space optical systems," *J. Lightw. Technol.*, vol. 38, no. 6, pp. 1286–1295, Mar. 2020.
- [24] H. AlQuwaiee, H.-C. Yang, and M.-S. Alouini, "On the asymptotic capacity of dual-aperture FSO systems with generalized pointing error model," *IEEE Trans. Wireless Commun.*, vol. 15, no. 9, pp. 6502–6512, Sep. 2016.
- [25] R. Boluda-Ruiz, A. García-Zambrana, C. Castillo-Vázquez, and B. Castillo-Vázquez, "Novel approximation of misalignment fading modeled by Beckmann distribution on free-space optical links," *Opt. Exp.*, vol. 24, no. 20, pp. 22635–22649, Oct. 2016.
- [26] A. A. Farid and S. Hranilovic, "Outage capacity optimization for free-space optical links with pointing errors," *J. Lightw. Technol.*, vol. 25, no. 7, pp. 1702–1710, Jul. 2007.
- [27] W. Gappmair, S. Hranilovic, and E. Leitgeb, "OOK performance for terrestrial FSO links in turbulent atmosphere with pointing errors modeled by Hoyt distributions," *IEEE Commun. Lett.*, vol. 15, no. 8, pp. 875–877, Aug. 2011.
- [28] F. Yang, J. Cheng, and T. A. Tsiftsis, "Free-space optical communication with nonzero boresight pointing errors," *IEEE Trans. Commun.*, vol. 62, no. 2, pp. 713–725, Feb. 2014.
- [29] O. S. Badarneh, R. Derbas, F. S. Almeahmadi, F. El Bouanani, and S. Muhaidat, "Performance analysis of FSO communications over \mathcal{F} turbulence channels with pointing errors," *IEEE Commun. Lett.*, vol. 25, no. 3, pp. 926–930, Mar. 2021.
- [30] M. Le-Tran and S. Kim, "Performance analysis of dual-hop FSO cooperative systems over \mathcal{F} turbulence with pointing errors," *Photon.*, vol. 9, no. 7, 2022, Art. no. 437.
- [31] J. Li, J. Q. Liu, and D. P. Taylor, "Optical communication using subcarrier PSK intensity modulation through atmospheric turbulence channels," *IEEE Trans. Commun.*, vol. 55, no. 8, pp. 1598–1606, Aug. 2007.
- [32] H. Samimi, "Optical communication using subcarrier intensity modulation through generalized turbulence channels," *J. Opt. Commun. Netw.*, vol. 4, no. 5, pp. 378–381, 2012.
- [33] W. O. Popoola and Z. Ghassemlooy, "BPSK subcarrier intensity modulated free-space optical communications in atmospheric turbulence," *J. Lightw. Technol.*, vol. 27, no. 8, pp. 967–973, Apr. 2009.
- [34] M. Niu, J. Cheng, and J. F. Holzman, "Error rate performance comparison of coherent and subcarrier intensity modulated optical wireless communications," *J. Opt. Commun. Netw.*, vol. 5, no. 6, pp. 554–564, 2013.
- [35] S. L. Cotton, "Human body shadowing in cellular device-to-device communications: Channel modeling using the shadowed κ - μ fading model," *IEEE J. Sel. Areas Commun.*, vol. 33, no. 1, pp. 111–119, Jan. 2015.
- [36] N. Vishwakarma and S. R., "On the maximal-ratio combining of FSO and RF links over generalized distributions and its applications in hybrid FSO/RF systems," *Opt. Commun.*, vol. 520, 2022, Art. no. 128542.
- [37] N. Vishwakarma and S. R., "Performance analysis of hybrid FSO/RF communication over generalized fading models," *Opt. Commun.*, vol. 487, 2021, Art. no. 126796.
- [38] M. D. Yacoub, "The $\alpha - \eta - \kappa - \mu$ fading model," *IEEE Trans. Antennas Propag.*, vol. 64, no. 8, pp. 3597–3610, Aug. 2016.
- [39] G. Alfano and A. De Maio, "Sum of squared shadowed-rice random variables and its application to communication systems performance prediction," *IEEE Trans. Wireless Commun.*, vol. 6, no. 10, pp. 3540–3545, Oct. 2007.
- [40] J. F. Paris, "Statistical characterization of κ - μ shadowed fading," *IEEE Trans. Veh. Technol.*, vol. 63, no. 2, pp. 518–526, Feb. 2014.
- [41] A. H. A. El-Malek, A. M. Salhab, S. A. Zummo, and M.-S. Alouini, "Effect of RF interference on the security-reliability tradeoff analysis of multiuser mixed RF/FSO relay networks with power allocation," *J. Lightw. Technol.*, vol. 35, no. 9, pp. 1490–1505, May 2017.
- [42] Z. Wang, W. Shi, and W. Liu, "Performance analysis of mixed RF/FSO system with CCI," *IET Commun.*, vol. 13, no. 14, pp. 2199–2206, 2019.
- [43] M. I. Petkovic, A. M. Cvetkovic, G. T. Djordjevic, and G. K. Karagiannidis, "Outage performance of the mixed RF/FSO relaying channel in the presence of interference," *Wireless Pers. Commun.*, vol. 96, no. 2, pp. 2999–3014, 2017.
- [44] S. B. Bambiwal, A. Upadhyay, R. S. Yaduvanshi, and V. K. Pandey, "Partial relay selection for combating the effects of co-channel interference in RF/FSO cooperative relaying," *Opt. Commun.*, vol. 475, 2020, Art. no. 126186.
- [45] O. M. S. Al-Ebraheemy, A. M. Salhab, M. El-Absi, S. A. Zummo, and S. S. Ikki, "Performance analysis of mixed interference aligned MIMO RF/unified FSO DF relaying with heterodyne detection and two IMDD models," *IEEE Access*, vol. 8, pp. 93297–93308, 2020.
- [46] A. Goel and R. Bhatia, "Joint impact of interference and hardware impairments on the performance of mixed RF/FSO cooperative relay networks," *Opt. Quantum Electron.*, vol. 53, no. 9, pp. 1–15, 2021.
- [47] I. S. Gradshteyn and I. M. Ryzhik, *Table of Integrals, Series, and Products*. New York, NY, USA: Academic Press, 2014.
- [48] F. J. Lopez-Martinez, J. F. Paris, and J. M. Romero-Jerez, "The κ - μ shadowed fading model with integer fading parameters," *IEEE Trans. Veh. Technol.*, vol. 66, no. 9, pp. 7653–7662, Sep. 2017.
- [49] A. Prudnikov, Y. A. Brychkov, and O. Marichev, *Integrals and Series Volume 3 : More Special Functions*. Oxford, U.K.: Taylor and Francis, 2003.
- [50] A. M. Mathai, R. K. Saxena, and H. J. Haubold, *The H-Function: Theory and Applications*. Berlin, Germany: Springer, 2009.
- [51] A. A. Kilbas, *H-Transforms: Theory and Applications*. Boca Raton, FL, USA: CRC Press, 2004.
- [52] M. O. Hasna and M.-S. Alouini, "A performance study of dual-hop transmissions with fixed gain relays," *IEEE Trans. Wireless Commun.*, vol. 3, no. 6, pp. 1963–1968, Nov. 2004.
- [53] H. Arezumand, H. Zamiri-Jafarian, and E. Soleimani-Nasab, "Outage and diversity analysis of underlay cognitive mixed RF-FSO cooperative systems," *J. Opt. Commun. Netw.*, vol. 9, no. 10, pp. 909–920, 2017.
- [54] Wolfram Research Inc., "The wolfram functions site," 2020. [Online]. Available: <http://functions.wolfram.com>
- [55] I. S. Ansari, S. Al-Ahmadi, F. Yilmaz, M.-S. Alouini, and H. Yanikomeroglu, "A new formula for the BER of binary modulations with dual-branch selection over generalized-K composite fading channels," *IEEE Trans. Commun.*, vol. 59, no. 10, pp. 2654–2658, Oct. 2011.
- [56] M. Abramowitz and I. A. Stegun, *Handbook of Mathematical Functions With Formulas, Graphs, and Mathematical Tables*, 10th ed. New York, NY, USA: Academic, 1972.
- [57] F. Yilmaz and M.-S. Alouini, "An MGF-based capacity analysis of equal gain combining over fading channels," in *Proc. IEEE 21st Annu. Int. Symp. Pers., Indoor Mobile Radio Commun.*, 2010, pp. 945–950.
- [58] P. Mittal and K. Gupta, "An Integral Involving Generalized Function of Two Variables," *Proc. Indian Acad. Sci.-Sect. A*, vol. 75, no. 3, pp. 117–123, 1972.